Geochemical Perspectives Letters

Ge, Te, and Zn isotopic link between Ryugu and CI chondrites

E. Wölfer[1*], J. Hellmann[1], C. Burkhardt[1], T. Kleine[1]

https://doi.org/10.7185/geochemlet.2537

Abstract

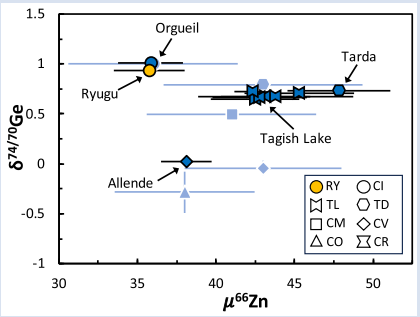

Analyses of samples returned from asteroid Ryugu have revealed chemical, mineralogical, and isotopic similarities to Ivuna-type (CI) carbonaceous chondrites. Compared to other carbonaceous chondrites, CI chondrites are characterised by heavy isotope enrichments of the moderately volatile elements, but until now no study demonstrated that this is also the case for Ryugu. Here we show that Ryugu and CI chondrites have similar elemental and mass dependent isotope systematics of the moderately volatile elements Ge, Te, and Zn, which are distinct from those of all other carbonaceous chondrites. The mass independent (nucleosynthetic) Zn isotope signatures of Ryugu are also most similar to CI chondrites, although the difference to other carbonaceous chondrites is not well resolved. Our results reinforce the notion that Ryugu and CI chondrites formed from the same precursor materials, and indicate that any processes acting on these materials before or after parent body accretion were similar. Given their similar chemical composition to the Sun, Ryugu/CI chondrites likely record the solar system's average chemical and mass dependent isotopic composition for moderately volatile elements.

Received 12 May 2025 | Accepted 15 August 2025 | Published 17 September 2025

Introduction

Japan Aerospace Exploration Agency's (JAXA) Hayabusa2 mission returned 5.4 g of sample of the Cb-type asteroid 162173 Ryugu to Earth (Tachibana *et al.*, 2022; Yada *et al.*, 2022). Initial analyses of the returned samples have revealed that Ryugu is petrologically, mineralogically, chemically, and isotopically similar to the Ivuna-type (CI) chondrites (Nakamura *et al.*, 2023; Yokoyama *et al.*, 2023a,b). These chondrites belong to the carbonaceous chondrites and with the exception of the highly volatile elements, their chemical composition closely resembles that of the solar photosphere. As such, CI chondrites are commonly taken to represent the bulk chemical composition of the solar system (*e.g.*, Palme and O'Neill, 2014). Compared to most other carbonaceous chondrites, CI chondrites are extremely rare, and owing to their friable nature, are susceptible to terrestrial alteration, which may have modified their compositions (*e.g.*, Bland *et al.*, 2006; Barrat *et al.*, 2012; Koefoed *et al.*, 2023). Thus, the returned samples from asteroid Ryugu provide the unique opportunity to examine CI chondrite-like material unaffected by terrestrial alteration.

Among the carbonaceous chondrites, CI chondrites exhibit unique nucleosynthetic isotope signatures for Fe and Ni (Hopp *et al.*, 2022; Spitzer *et al.*, 2024) and also show distinct mass dependent isotope compositions for the moderately volatile elements (MVEs; those that condense from a solar gas between ~1250 and 650 K). However, while Ryugu and Orgueil, the most commonly analysed CI chondrite, have indistinguishable mass dependent isotopic composition of the MVEs Zn (Paquet *et al.*, 2023) and K (Hu *et al.*, 2024), these compositions also overlap with those of other volatile-rich carbonaceous chondrites and, therefore, do not provide a clear link between CI chondrites and Ryugu. Moreover, while Ryugu samples exhibit nucleosynthetic Zn isotope anomalies similar to CI chondrites, these compositions overlap with those of other carbonaceous chondrites (Paquet *et al.*, 2023). Given these ambiguities, it is important to assess whether there are other MVEs having isotopic signatures that would provide a link between CI chondrites and Ryugu, and allow distinguishing these materials from other carbonaceous chondrites. This is important for fully understanding the chemical and isotopic make-up of asteroid Ryugu, the nature of the processes determining compositional variations among CI chondrite-like materials, and, ultimately, the use of these materials to determine the bulk chemical composition of the solar system.

The two MVEs Ge and Te hold considerable promise to reveal compositional signatures that link Ryugu to CI chondrites and distinguish them from other carbonaceous chondrites. Both elements have been shown to display large and systematic mass dependent isotopic variations among the carbonaceous chondrites, where CI chondrites are characterised by the highest Ge and Te concentrations and strongest heavy isotope enrichments (Hellmann *et al.*, 2020; Wölfer *et al.*, 2025a). Given the strong genetic and chemical link between Ryugu and CI chondrites, Ryugu is expected to exhibit similarly distinct Ge and Te isotope systematics. To assess as to whether this is the case, we report Ge and Te isotope data for a single Ryugu sample together with data for several other MVE-rich carbonaceous chondrites. To facilitate direct comparison to the MVE Zn, all samples have also been analysed for their Zn isotope compositions.

1. Max Planck Institute for Solar System Research, Justus-von-Liebig-Weg 3, 37077 Göttingen, Germany
* Corresponding author (email: woelfer@mps.mpg.de)

Samples and Methods

We analysed a 12.4 mg Ryugu sample from chamber A (A0220) together with equivalent masses of Orgueil and the ungrouped C2 chondrites Tarda and Tagish Lake. To test the reproducibility of the isotope measurements on such small sample masses, and to assess the magnitude of any potential heterogeneity at the ~12 mg level, six aggregate samples of Tagish Lake, each weighing ~12–15 mg, were also analysed. Similar to CI chondrites and Ryugu, Tagish Lake is dominated by fine grained, volatile-rich matrix with only very low abundances of chondrules, refractory inclusions, and FeNi metal (*e.g.*, Alexander, 2019), making this sample suitable to assess the effect of any potential sample heterogeneity on the elemental and isotopic compositions of MVEs in matrix-rich carbonaceous chondrites. The Orgueil sample analysed in this study is an aliquot from a ~0.7 g powder prepared in a prior study (Schneider *et al.*, 2023). Finally, for direct comparison we also analysed aliquots of the large, homogenised MS-A powder of the CV3 chondrite Allende, which has previously been analysed for Ge and Te isotopes using the same analytical setup as in this study (Hellmann *et al.*, 2020; Wölfer *et al.*, 2025a).

The sample digestion, chemical separation and isotope measurements of Ge, Te, and Zn followed our previously established procedures (Hellmann *et al.*, 2020; Steller *et al.*, 2022; Wölfer *et al.*, 2025a,b) and are described in the Supplementary Information. For Ge and Te, the instrumental mass bias was corrected using ^{70}Ge–^{73}Ge (Wölfer *et al.*, 2025b) and ^{123}Te–^{125}Te double spikes (Hellmann *et al.*, 2020), and the data are reported as the per mille deviations from certified standard solutions (see Table 1 for definitions). The double spike measurements also provide precise Ge and Te concentrations determined by isotope dilution. No double spike was used for Zn, and the instrumental mass bias was corrected by standard sample bracketing. This has the advantage that for Zn we can also report mass independent isotope variations (*i.e.* nucleosynthetic isotope anomalies) after internal normalisation of the data. As for Ge and Te, the mass dependent Zn isotope data are reported as the per mille deviations from a certified standard solution, while the nucleosynthetic isotope anomalies are given as the ppm deviations from the standard after internal normalisation to either ^{68}Zn/^{64}Zn or ^{67}Zn/^{64}Zn.

Results

The Ge, Te, and Zn concentrations and isotopic compositions of Ryugu (A0220) and the carbonaceous chondrites investigated in this study are provided in Table 1. We show in the SI (Tables S-1 to S-3, Fig. S-1) that the new data for Orgueil, Tagish Lake, Tarda, and Allende agree well with results of prior studies, demonstrating that the combined use of two different double spikes has no effect on the isotope analyses of any of the three elements investigated, and that analysing mg-sized samples does not compromise the accuracy and precision of the isotopic data. While the six Tagish Lake subsamples have similar Ge, Te, and Zn concentrations and isotopic compositions, they show resolved $\delta^{74/70}$Ge and $\delta^{66/64}$Zn variations, indicating some level of compositional heterogeneities at the ~12 mg sampling scale (Fig. S-2). This heterogeneity appears to be more pronounced for Zn, where our analyses of several samples of Tagish Lake are systematically offset from some prior analyses (Fig. S-2).

Ryugu sample A0220 and Orgueil have the highest Ge, Te, and Zn concentrations and are characterised by the most elevated $\delta^{74/70}$Ge and $\delta^{128/126}$Te values among the carbonaceous chondrites of this and prior studies (Figs. 1, S-3). Consistent with Paquet *et al.* (2023), we find no $\delta^{66/64}$Zn differences among Ryugu sample A0220, Orgueil, Tagish Lake, and Tarda, despite their different Zn contents. Compared to CI chondrites, Ryugu sample A0220 is enriched in Ge, Te, and Zn by ~5–10 %, consistent with the ~10 % higher Zn concentrations found in prior studies (Paquet *et al.*, 2023; Yokoyama *et al.*, 2023a). These higher MVE concentrations can partly or wholly be accounted for by the >6 wt. % lower water content of Ryugu samples compared to CI chondrites, and ultimately might stem from the incorporation of terrestrial water into CI meteorites and/or the loss of water from Ryugu's surface during space weathering (Noguchi *et al.*, 2023; Yokoyama *et al.*, 2023a). For Ge, the $\delta^{74/70}$Ge of sample A0220 is ~0.07 ‰ lower than for Orgueil samples analysed in this and previous studies. This difference is similar to those found among the subsamples of Tagish Lake, indicating these differences most likely reflect sample heterogeneity. This is likely also the case for Te, where sample A0220 has the same $\delta^{128/126}$Te as Ivuna (Hellmann *et al.*, 2020), but a slightly lower $\delta^{128/126}$Te than two analyses of Orgueil (from this study and Hellmann *et al.*, 2020).

For the nucleosynthetic Zn isotope anomalies, sample A0220, together with the other carbonaceous chondrites of this study, plots in the CC field on μ^{66}Zn–μ^{68}Zn and μ^{66}Zn–μ^{67}Zn diagrams (Fig. 2). The results for Orgueil, Tagish Lake, Tarda, and Allende agree well with those of prior studies. Ryugu sample A0220 is characterised by $\mu^{66}\text{Zn} = 36 \pm 2$, identical to the values measured for Orgueil in this study and by Steller *et al.* (2022) (the latter data have been corrected for a small –9 ppm offset measured for terrestrial samples). The only other study on Zn isotope anomalies in Ryugu only reported μ^{66}Zn values using the ^{68}Zn/^{64}Zn normalisation (Paquet *et al.*, 2023), which results in overall smaller anomalies than the ^{67}Zn/^{64}Zn normalisation. These authors found a mean $\mu^{66}\text{Zn} = 33 \pm 4$ (2 s.e.) for samples from chambers A and C, slightly higher than $\mu^{66}\text{Zn} = 27 \pm 1$ (95 % conf.) (^{68}Zn/^{64}Zn normalisation) measured here.

Discussion

A genetic link between asteroid Ryugu and CI chondrites has been established in numerous studies, based on for instance nucleosynthetic isotope anomalies in the non-volatile elements Cr, Ti, Fe, and Ni (Hopp *et al.*, 2022; Yokoyama *et al.*, 2023a, 2023b; Spitzer *et al.*, 2024). Among the MVEs, Zn also shows nucleosynthetic isotope anomalies, but until now no isotopic variations among the carbonaceous chondrites have been identified (Savage *et al.*, 2022; Steller *et al.*, 2022; Martins *et al.*, 2023). However, the data of this study suggest that CI chondrites and Ryugu may have distinct nucleosynthetic Zn isotope signatures compared to other carbonaceous chondrites. We find identical μ^{66}Zn values for two separate analyses of Orgueil ($\mu^{66}\text{Zn} = 36 \pm 5$ in Steller *et al.*, 2022, and 36 ± 2 in this study) and Ryugu sample A0220 ($\mu^{66}\text{Zn} = 36 \pm 2$). By contrast, for the next most volatile-rich carbonaceous chondrites, Tagish Lake and Tarda, we find more elevated μ^{66}Zn values of 43 ± 2 and 48 ± 3, respectively (Table 1). This suggests that CI chondrites/Ryugu may be characterised by slightly lower μ^{66}Zn values than other volatile-rich carbonaceous chondrites. This difference is barely resolved, however, and there are other non-CI carbonaceous chondrites overlapping with the μ^{66}Zn values of CI chondrites and Ryugu (Fig. 2). As such, additional high precision Zn isotope data are needed for firmly establishing a nucleosynthetic Zn isotope difference between CI and other carbonaceous chondrites.

More robust evidence for an MVE-based link between Ryugu and CI chondrites comes from the elemental and mass dependent isotopic compositions reported here. Compositional

Table 1 Germanium, Te, and Zn concentration and isotopic data for Ryugu (A0220) and carbonaceous chondrites.

Sample	Weight (mg)	Ge (μg/g) (±2σ)	*n* (Ge)	$\delta^{74/70}$Ge (±95 % CI)	Te (ng/g) (±2σ)	*n* (Te)	$\delta^{128/126}$Te (±2 s.d.)	Zn (μg/g)	*n* (Zn)	$\delta^{66/64}$Zn (±2 s.d.)	μ^{66}Zn (±95 % CI)	μ^{68}Zn (±95 % CI)	μ^{66}Zn (±95 % CI)	μ^{68}Zn (±95 % CI)
											^{67}Zn/^{64}Zn int. norm.		^{68}Zn/^{64}Zn int. norm.	
Ryugu (A0220)	12.4	37.2 ± 0.2	12	0.93 ± 0.03	2372 ± 8	3	0.13 ± 0.03	348	14	0.51 ± 0.12	36 ± 2	16 ± 4	27 ± 1	–12 ± 3
Orgueil (CI)	12.7	33.9 ± 0.2	12	1.01 ± 0.03	2269 ± 7	3	0.15 ± 0.02	318	10	0.51 ± 0.08	36 ± 2	16 ± 6	28 ± 2	–12 ± 4
Orgueil (CI)[a]	7.9							298	16	0.53 ± 0.11	36 ± 5	14 ± 9	28 ± 3	–10 ± 7
Tagish Lake (C2 ung.)	11.5	25.6 ± 0.3	9	0.67 ± 0.03	1729 ± 6	3	0.13 ± 0.03	196	8	0.51 ± 0.08	43 ± 3	21 ± 5	33 ± 2	–16 ± 3
Tagish Lake (C2 ung.)	11.6	25.2 ± 0.3	9	0.65 ± 0.03	1764 ± 6	3	0.12 ± 0.03	202	8	0.63 ± 0.05	42 ± 3	18 ± 4	33 ± 1	–13 ± 3
Tagish Lake (C2 ung.)	12.5	25.1 ± 0.3	9	0.66 ± 0.04	1556 ± 5	4	0.12 ± 0.06	188	8	0.52 ± 0.04	43 ± 3	19 ± 6	34 ± 3	–14 ± 5
Tagish Lake (C2 ung.)	11.7	25.5 ± 0.3	9	0.67 ± 0.02	1647 ± 5	3	0.10 ± 0.01	187	8	0.57 ± 0.06	44 ± 5	20 ± 9	34 ± 2	–15 ± 7
Tagish Lake (C2 ung.)	14.8	26.2 ± 0.3	9	0.71 ± 0.03	1756 ± 6	4	0.12 ± 0.05	197	8	0.53 ± 0.09	45 ± 3	20 ± 4	35 ± 3	–15 ± 3
Tagish Lake (C2 ung.)	13.3	25.5 ± 0.3	9	0.72 ± 0.02	1691 ± 6	4	0.11 ± 0.03	188	6	0.48 ± 0.03	42 ± 1	17 ± 6	33 ± 2	–13 ± 5
Mean (2 s.d., *n* = 6)		**25.5 ± 0.8**		**0.68 ± 0.06**	**1690 ± 157**		**0.12 ± 0.02**	**193**		**0.54 ± 0.10**	**43 ± 2**	**19 ± 3**	**33 ± 2**	**–14 ± 3**
Wt. mean (IsoplotR)		**25.4 ± 0.1**		**0.69 ± 0.02**	**1679 ± 67**		**0.11 ± 0.01**	**193**		**0.53 ± 0.02**	**42 ± 1**	**19 ± 2**	**33 ± 1**	**–15 ± 2**
Tarda (C2 ung.)	16.3	24.4 ± 0.2	4	0.73 ± 0.03	1622 ± 5	3	0.07 ± 0.07	194	9	0.54 ± 0.05	48 ± 3	25 ± 5	35 ± 2	–19 ± 4
Tarda (C2 ung.) [a]	13.0							205	15	0.46 ± 0.06	43 ± 6	21 ± 7	31 ± 6	–16 ± 6
J. Winselwan (CM) [a]	17.9							183	20	0.41 ± 0.08	41 ± 5	19 ± 11	31 ± 2	–14 ± 8
Allende (CV)	102.9	17.2 ± 0.2	6	0.02 ± 0.03	954 ± 3	4	0.02 ± 0.02	111	25	0.31 ± 0.07	38 ± 2	15 ± 2	31 ± 1	–11 ± 2
Allende (CV) [a]	74.3							108	68	0.27 ± 0.08	43 ± 3	19 ± 6	32 ± 1	–15 ± 4
Vigarano (CV) [a]	30.2							104	15	0.17 ± 0.05	43 ± 4	15 ± 8	35 ± 2	–11 ± 6
Kainsaz (CO) [a]	28.7							94	18	0.38 ± 0.05	38 ± 4	17 ± 7	30 ± 3	–12 ± 5

The Ge and Te concentrations were determined by isotope dilution and the Zn concentrations were determined by quadrupole ICP–MS, the latter of which have an uncertainty of ~5 %. The isotope data of individual samples are reported as the mean of pooled measurements and are expressed as in the common δ notation as δ^{74}Ge [‰] = $[(^{74}Ge/^{70}Ge)_{sample}/(^{74}Ge/^{70}Ge)_{SRM3210a} - 1] \times 10^3$, δ^{128}Te [‰] = $[(^{128}Te/^{126}Te)_{sample}/(^{128}Te/^{126}Te)_{SRM3156} - 1] \times 10^3$, δ^{66}Zn [‰] = $[(^{66}Zn/^{64}Zn)_{sample}/(^{66}Zn/^{64}Zn)_{JMC,Lyon} - 1] \times 10^3$, and μ^{i}Zn = $[(^{i}Zn/^{64}Zn)_{sample}/(^{i}Zn/^{64}Zn)_{SRM683} - 1] \times 10^6$, respectively. n: number of isotope analyses.

[a] Mass independent Zn isotope data previously published in Steller *et al.* (2022).

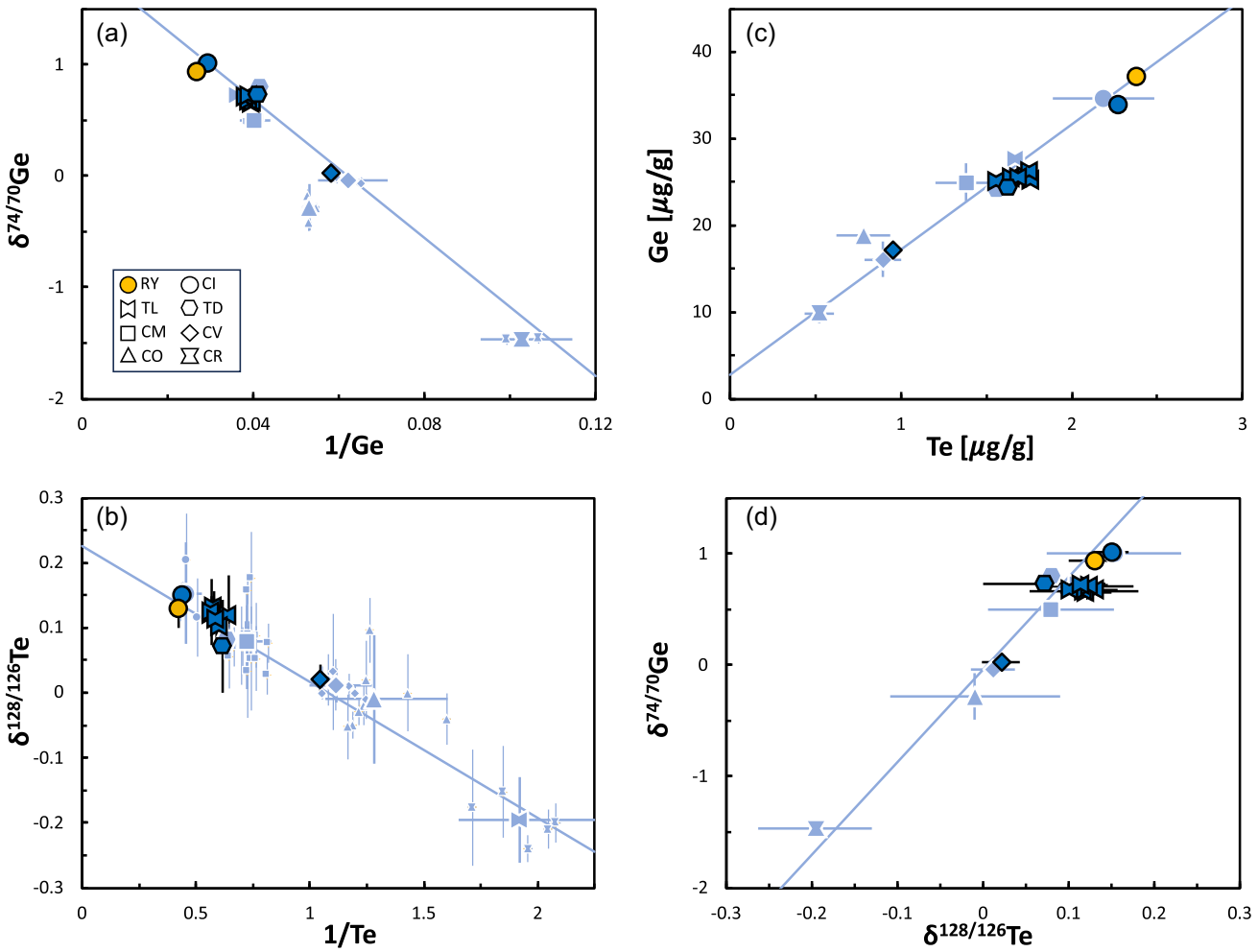

Figure 1 Diagrams of **(a)** Ge concentration *vs.* $\delta^{74/70}$Ge, **(b)** Te concentration *vs.* $\delta^{128/126}$Te, **(c)** Te *vs.* Ge concentrations, and **(d)** $\delta^{128/126}$Te *vs.* $\delta^{74/70}$Ge for carbonaceous chondrites (data from this study in dark blue; literature data in light blue [small symbols represent individual samples; large symbols represent group averages]). Ryugu sample A0220 is plotted as orange circle. Literature data for Ge is from Wölfer *et al.* (2025a); data for Te is from Hellmann *et al.* (2020, 2023) and Morton *et al.* (2024). The data of Morton *et al.* (2024) are re-normalised to $\delta^{128/126}$Te and the SRM standard used by Hellmann *et al.* (2020, 2023). Linear regressions calculated using IsoplotR based on group averages.

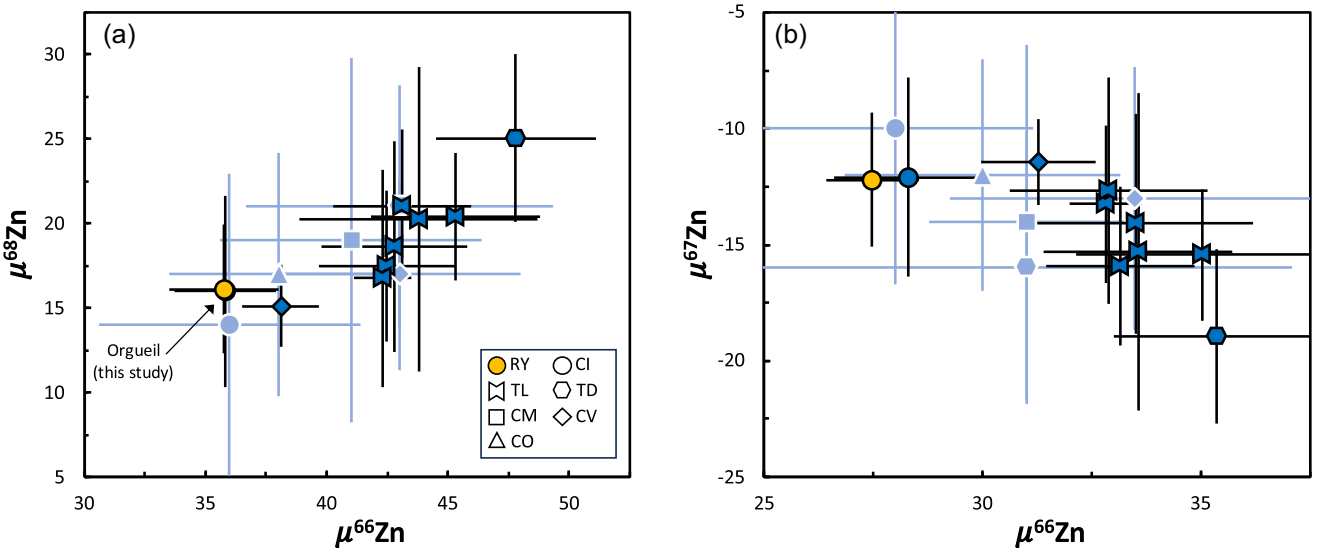

Figure 2 **(a)** μ^{66}Zn *vs.* μ^{68}Zn and **(b)** μ^{66}Zn *vs.* μ^{67}Zn diagrams for carbonaceous chondrites. Symbols as in Figure 1. Ryugu sample A0220 plots within the CC field and, together with CI chondrites, is characterised by slightly smaller μ^{i}Zn values compared to Tarda and Tagish Lake. Literature data from Steller *et al.* (2022).

variations among the carbonaceous chondrites are thought to reflect mixing among the chondrite's constituent components, namely volatile-poor, isotopically light chondrules and volatile-rich, isotopically heavy, CI chondrite-like matrix (*e.g.*, Alexander, 2019; Hellmann *et al.*, 2020). Variations in the abundance of these two components result in correlations among the concentrations and mass dependent isotopic compositions of the MVEs, including Ge (Wölfer *et al.*, 2025a), Te (Hellmann *et al.*, 2020), Zn (*e.g.*, Pringle *et al.*, 2017), Rb (*e.g.*, Nie *et al.*, 2021), K (*e.g.*, Koefoed *et al.*, 2023), and Cd (Morton *et al.*, 2024). Our results are consistent with these correlations and demonstrate that Ryugu and Orgueil together are characterised by distinctly higher MVE abundances and heavier isotopic compositions compared to other carbonaceous chondrites (Fig. 1). However, given the small mass analysed for each sample, it is important to assess how much of the observed variability may reflect sample heterogeneities rather than true compositional variations among the chondrite groups. For instance, different Ryugu subsamples exhibit variable Cr, Ti, and Ni nucleosynthetic isotope signatures (Yokoyama *et al.*, 2023a, 2023b; Spitzer *et al.*, 2024), which at least in part have been attributed to the redistribution of isotopically anomalous phases during aqueous alteration in the parent body (Yokoyama *et al.*, 2023b). The pronounced Mo isotope anomalies observed for a Ryugu sample has been explained in a similar manner (Nakanishi *et al.*, 2023). These observations suggest that small scale heterogeneities may also exist for mass dependent isotope compositions. For instance, mass dependent Zn isotope variations have been observed among the components of chondrites (Luck *et al.*, 2005; Pringle *et al.*, 2017), and so over- or under-sampling of certain components having distinct isotopic compositions may have occurred.

Our results for six ~12–15 mg subsamples of Tagish Lake show that the effects of sample heterogeneity are different for Ge, Te, and Zn. While the $\delta^{128/126}$Te values are quite homogeneous, $\delta^{74/70}$Ge and $\delta^{66/64}$Zn values vary by ~0.07 ‰ and ~0.16 ‰, respectively. For Zn this difference covers almost half of the entire $\delta^{66/64}$Zn variations observed among carbonaceous chondrites. By contrast, for Ge, these variations amount to only ~3 % of the overall $\delta^{74/70}$Ge variability among the carbonaceous chondrites (Wölfer *et al.*, 2025a), and the difference between CI chondrites and Tagish Lake itself is about four times larger than the heterogeneity observed among the CI chondrite and Ryugu samples. These observations suggest that the disparate levels of isotopic heterogeneity among the Tagish Lake subsamples are neither controlled by volatility (because Te and Zn have similar condensation temperatures) nor by heterogeneous sampling of chondrule and matrix fractions (because in this case similar relative variations would be expected for all three elements). Instead, they more likely reflect differences in the mobility of these elements during parent body alteration, and in the magnitude of isotope fractionation among the MVE's host minerals. Regardless of their exact cause, the larger intra-sample $\delta^{66/64}$Zn variability combined with the overall smaller range of $\delta^{66/64}$Zn values among carbonaceous chondrites makes Zn less suitable for linking Ryugu samples to a specific carbonaceous chondrite group than Ge and Te. Moreover, the larger overall isotope fractionation of Ge compared to Te makes mass dependent Ge isotope variations particularly powerful to identify genetic relations of MVEs among carbonaceous chondrite-like materials, especially for the small sample sizes typically available from sample return missions.

The Ge and Te results of this study demonstrate that compared to other carbonaceous chondrites, Ryugu and CI chondrites are characterised by elemental and heavy isotope enrichments in the MVEs. The same conclusion was reached previously based on Zn isotopes (Paquet *et al.*, 2023), but we emphasise that only for Ge and Te are the isotopic compositions of Ryugu and CI chondrites distinct from those of other volatile-rich carbonaceous chondrites.

Identical nucleosynthetic isotope signatures of Ryugu and CI chondrites have revealed that both formed from the same mix of presolar and nebular materials, but these signatures provide little information on any physicochemical processes acting on these materials before and after parent body accretion. The mass dependent isotopic compositions of MVEs are a more sensitive tracer of such processes, and so the MVE-based link between Ryugu and CI chondrites indicates that any physicochemical processes acting on these materials were also similar. Given the strong chemical similarities between Ryugu/CI chondrites and the solar photosphere, this in turn implies that these samples are good proxies for the average chemical and mass dependent isotopic compositions of the MVEs for most of the solar protoplanetary disk and, hence, the bulk solar system. Importantly, as is evident for instance from the distinct O isotope composition of the Sun (McKeegan *et al.*, 2011) for mass independent isotope anomalies, the isotopic composition of the solar system may be markedly different from that of CI chondrites, which likely was established by mixing of isotopically distinct materials during the formation and dynamical evolution of the protoplanetary disk (*e.g.*, Nanne *et al.*, 2019).

Acknowledgements

The Ryugu samples used in this paper were distributed through The Announcement of Opportunity for Hayabusa2 samples. These samples were referred to the Ryugu Sample Database at https://www.darts.isas.jaxa.jp/curation/hayabusa2/. We gratefully acknowledge Rayssa Martins and Kun Wang for their constructive comments and Helen Williams for her editorial handling. This work was funded by the European Research Council Advanced Grant HolyEarth (grant no. 101019380).

Editor: Helen Williams

Additional Information

Supplementary Information accompanies this letter at https://www.geochemicalperspectivesletters.org/article2537.

Cite this letter as: Wölfer, E., Hellmann, J., Burkhardt, C., Kleine, T. (2025) Ge, Te, and Zn isotopic link between Ryugu and CI chondrites. *Geochem. Persp. Let.* 37, 1–6. https://doi.org/10.7185/geochemlet.2537

References

Alexander, C.M.O'D. (2019) Quantitative models for the elemental and isotopic fractionations in chondrites: The carbonaceous chondrites. *Geochimica et Cosmochimica Acta* 254, 277–309. https://doi.org/10.1016/j.gca.2019.02.008

Barrat, J.A., Zanda, B., Moynier, F., Bollinger, C., Liorzou, C., Bayon, G. (2012) Geochemistry of CI chondrites: Major and trace elements, and Cu and Zn Isotopes. *Geochimica et Cosmochimica Acta* 83, 79–92. https://doi.org/10.1016/j.gca.2011.12.011

Bland, P.A., Zolensky, M.E., Benedix, G.K., Sephton, M.A. (2006) Weathering of Chondritic Meteorites. In: Lauretta, D.S., McSween, H.Y. (Eds.) *Meteorites and the Early Solar System II*. University of Arizona Press, Tucson, 853–868. https://doi.org/10.2307/j.ctv1v7zdmm.45

Hellmann, J.L., Hopp, T., Burkhardt, C., Kleine, T. (2020) Origin of volatile element depletion among carbonaceous chondrites. *Earth and Planetary Science Letters* 549, 116508. https://doi.org/10.1016/j.epsl.2020.116508

Hellmann, J.L., Schneider, J.M., Wölfer, E., Drążkowska, J., Jansen, C.A., Hopp, T., Burkhardt, C., Kleine, T. (2023) Origin of Isotopic Diversity among Carbonaceous Chondrites. *The Astrophysical Journal Letters* 946, L34. https://doi.org/10.3847/2041-8213/acc102

Hopp, T., Dauphas, N., Abe, Y., Aléon, J., Alexander, C.M.O'D. *et al.* (2022) Ryugu's nucleosynthetic heritage from the outskirts of the Solar System. *Science Advances* 8, eadd8141. https://doi.org/10.1126/sciadv.add8141

Hu, Y., Moynier, F., Dai, W., Paquet, M., Yokoyama, T. *et al.* (2024) Pervasive aqueous alteration in the early Solar System revealed by potassium isotopic variations in Ryugu samples and carbonaceous chondrites. *Icarus* 409, 115884. https://doi.org/10.1016/j.icarus.2023.115884

Koefoed, P., Barrat, J.-A., Pravdivtseva, O., Alexander, C.M.O'D., Lodders, K., Ogliore, R., Wang, K. (2023) The potassium isotopic composition of CI chondrites and the origin of isotopic variations among primitive planetary bodies. *Geochimica et Cosmochimica Acta* 358, 49–60. https://doi.org/10.1016/j.gca.2023.07.025

Luck, J.-M., Othman, D.B., Albarède, F. (2005) Zn and Cu isotopic variations in chondrites and iron meteorites: Early solar nebula reservoirs and parent-body processes. *Geochimica et Cosmochimica Acta* 69, 5351–5363. https://doi.org/10.1016/j.gca.2005.06.018

Martins, R., Kuthning, S., Coles, B.J., Kreissig, K., Rehkämper, M. (2023) Nucleosynthetic isotope anomalies of zinc in meteorites constrain the origin of Earth's volatiles. *Science* 379, 369–372. https://doi.org/10.1126/science.abn1021

McKeegan, K.D., Kallio, A.P.A., Heber, V.S., Jarzebinski, G., Mao, P.H., Coath, C.D., Kunihiro, T., Wiens, R.C., Nordholt, J.E., Moses Jr., R.W., Reisenfeld, D.B., Jurewicz, A.J.G., Burnett, D.S. (2011) The Oxygen Isotopic Composition of the Sun Inferred from Captured Solar Wind. *Science* 332, 1528–1532. https://doi.org/10.1126/science.1204636

Morton, E.M., Pickard, H., Wombacher, F., Huang, Y., Palk, E., Martins, R., Kuthning, S., Schönbächler, M., Rehkämper, M. (2024) Volatile Element Depletion of Carbonaceous Chondrites—Insights from Mass-dependent Zinc, Cadmium, and Tellurium Isotope Variations. *The Astrophysical Journal* 977, 53. https://doi.org/10.3847/1538-4357/ad87ed

Nakamura, T., Matsumoto, M., Amano, K., Enokido, Y., Zolensky, M.E. *et al.* (2023) Formation and evolution of carbonaceous asteroid Ryugu: Direct evidence from returned samples. *Science* 379, eabn8671. https://doi.org/10.1126/science.abn8671

Nakanishi, N., Yokoyama, T., Ishikawa, A., Walker, R.J., Abe, Y. *et al.* (2023) Nucleosynthetic *s*-Process Depletion in Mo from Ryugu samples returned by Hayabusa2. *Geochemical Perspectives Letters* 28, 31–36. https://doi.org/10.7185/geochemlet.2341

Nanne, J.A.M., Nimmo, F., Cuzzi, J.N., Kleine, T. (2019) Origin of the non-carbonaceous–carbonaceous meteorite dichotomy. *Earth and Planetary Science Letters* 511, 44–54. https://doi.org/10.1016/j.epsl.2019.01.027

Nie, N.X., Chen, X.-Y., Hopp, T., Hu, J.Y., Zhang, Z.J., Teng, F.-Z., Shahar, A., Dauphas, N. (2021) Imprint of chondrule formation on the K and Rb isotopic compositions of carbonaceous meteorites. *Science Advances* 7, eabl3929. https://doi.org/10.1126/sciadv.abl3929

Noguchi, T., Matsumoto, T., Miyake, A., Igami, Y., Haruta, M. *et al.* (2023) A dehydrated space-weathered skin cloaking the hydrated interior of Ryugu. *Nature Astronomy* 7, 170–181. https://doi.org/10.1038/s41550-022-01841-6

Palme, H., O'Neill, H.St.C. (2014) 3.1 - Cosmochemical Estimates of Mantle Composition. In: Holland, H.D., Turekian, K.K. (Eds.) *Treatise on Geochemistry*. Second Edition, Elsevier, Amsterdam, 1–39. https://doi.org/10.1016/B978-0-08-095975-7.00201-1

Paquet, M., Moynier, F., Yokoyama, T., Dai, W., Hu, Y. *et al.* (2023) Contribution of Ryugu-like material to Earth's volatile inventory by Cu and Zn isotopic analysis. *Nature Astronomy* 7, 182–189. https://doi.org/10.1038/s41550-022-01846-1

Pringle, E.A., Moynier, F., Beck, P., Paniello, R., Hezel, D.C. (2017) The origin of volatile element depletion in early solar system material: Clues from Zn isotopes in chondrules. *Earth and Planetary Science Letters* 468, 62–71. https://doi.org/10.1016/j.epsl.2017.04.002

Savage, P.S., Moynier, F., Boyet, M. (2022) Zinc isotope anomalies in primitive meteorites identify the outer solar system as an important source of Earth's volatile inventory. *Icarus* 386, 115172. https://doi.org/10.1016/j.icarus.2022.115172

Schneider, J.M., Burkhardt, C., Kleine, T. (2023) Distribution of *s*-, *r*-, and *p*-process Nuclides in the Early Solar System Inferred from Sr Isotope Anomalies in Meteorites. *The Astrophysical Journal Letters* 952, L25. https://doi.org/10.3847/2041-8213/ace187

Spitzer, F., Kleine, T., Burkhardt, C., Hopp, T., Yokoyama, T. *et al.* (2024) The Ni isotopic composition of Ryugu reveals a common accretion region for carbonaceous chondrites. *Science Advances* 10, eadp2426. https://doi.org/10.1126/sciadv.adp2426

Steller, T., Burkhardt, C., Yang, C., Kleine, T. (2022) Nucleosynthetic zinc isotope anomalies reveal a dual origin of terrestrial volatiles. *Icarus* 386, 115171. https://doi.org/10.1016/j.icarus.2022.115171

Tachibana, S., Sawada, H., Okazaki, R., Takano, Y., Sakamoto, K. *et al.* (2022) Pebbles and sand on asteroid (162173) Ryugu: In situ observation and particles returned to Earth. *Science* 375, 1011–1016. https://doi.org/10.1126/science.abj8624

Wölfer, E., Burkhardt, C., Nimmo, F., Kleine, T. (2025a) Origin of moderately volatile elements in Earth inferred from mass-dependent Ge isotope variations among chondrites. *Earth and Planetary Science Letters* 663, 119435. https://doi.org/10.1016/j.epsl.2025.119435

Wölfer, E., Burkhardt, C., Kleine, T. (2025b) Germanium stable isotope measurements by double-spike MC-ICPMS. *Journal of Analytical Atomic Spectrometry* 40, 1023–1036. https://doi.org/10.1039/D4JA00359D

Yada, T., Abe, M., Okada, T., Nakato, A., Yogata, K. *et al.* (2022) Preliminary analysis of the Hayabusa2 samples returned from C-type asteroid Ryugu. *Nature Astronomy* 6, 214–220. https://doi.org/10.1038/s41550-021-01550-6

Yokoyama, T., Nagashima, K., Nakai, I., Young, E.D., Abe, Y. *et al.* (2023a) Samples returned from the asteroid Ryugu are similar to Ivuna-type carbonaceous meteorites. *Science* 379, eabn7850. https://doi.org/10.1126/science.abn7850

Yokoyama, T., Wadhwa, M., Iizuka, T., Rai, V., Gautam, I. *et al.* (2023b) Water circulation in Ryugu asteroid affected the distribution of nucleosynthetic isotope anomalies in returned sample. *Science Advances* 9, eadi7048. https://doi.org/10.1126/sciadv.adi7048

Ge, Te, and Zn isotopic link between Ryugu and CI chondrites

E. Wölfer, J. Hellmann, C. Burkhardt, T. Kleine

Supplementary Information

The Supplementary Information includes:

- Extended Methods
- Tables S-1 to S-4
- Figures S-1 to S-3
- Supplementary Information References

Extended Methods

Sample Preparation and Chemical Separation of Ge, Te, and Zn

A total sample mass of ~5.4 g was collected from asteroid Ryugu and returned by the Hayabusa2 spacecraft (Tachibana *et al.*, 2022; Yada *et al.*, 2022). For this study, a subsample from sample chamber A (12.4 mg; A0220) was newly digested for combined Ge, Te, and Zn isotope analyses. To test our analytical protocol for limited sample quantities, we also digested small aliquots of Orgueil and Tarda (10–20 mg) that were taken from homogeneous bulk powders obtained from >1 g pieces (Hellmann *et al.*, 2020, 2023; Schneider *et al.*, 2023). Moreover, a ~100 mg powder aliquot of Allende was taken from a homogenous bulk powder obtained from a ~100 g piece (Hellmann *et al.*, 2020). Finally, to test for isotopic variability in CC chondrite samples on the scale of only a few mg, we carefully removed six aliquots from different domains of a large hand piece of Tagish Lake (10–15 mg, respectively).

For all samples, the (powdered) bulk rock aliquots were weighed into 60 ml Savillex PFA vials, mixed with appropriate amounts of both, a ^{70}Ge–^{73}Ge double spike (Wölfer *et al.*, 2025b), as well as a ^{123}Te–^{125}Te double spike (Hellmann *et al.*, 2020). The samples were digested on a hot-plate (120 °C, 5 days) using a (2:1) mixture of conc. HF-HNO_3. After digestion, the samples were evaporated and re-dissolved multiple times in concentrated HNO_3 at 120 °C to fume off fluorides, and ensure complete sample dissolution and sample-spike equilibration. The samples were then dried down twice in 1 M HF and finally re-dissolved in 2 ml 1 M HF in preparation for ion exchange chromatography. Fluorides that may have formed again during this step, were centrifuged and separated (see below).

In a first step, Ge was separated from the silicate matrices via a two-stage ion exchange chemistry broadly following previously established protocols (Luais, 2007, 2012; Wölfer *et al.* 2025b). The samples were loaded in 2 ml 1 M HF onto Bio-Rad columns filled with 2 ml of pre-cleaned and conditioned Bio-Rad AG 1-X8 anion exchange resin (200–400 mesh; Allende was split on three columns), and most matrix elements, including Zn (~100 %) and large parts of the Te (~80 %), were washed off by additional 13 ml 1 M HF, 2 ml H_2O, and 4 ml 0.2 M HNO_3. By contrast, Ge

together with the remaining Te (~20 %) remained on the resin and were subsequently eluted in 20 ml 0.2 M HNO_3. Germanium was then separated from Te and some remaining matrix elements using Bio-Rad columns filled with 2 ml of pre-cleaned and conditioned Bio-Rad AG 50W-X8 cation exchange resin (200–400 mesh). Sample solutions were loaded in 2 ml 0.5 M HNO_3 and Ge was directly eluted by additional 8 ml 0.5 M HNO_3, whereas Te and the remaining matrix elements remained on the resin and were subsequently washed off by 10 ml 1 M HNO_3 and 10 ml 6 M HCl. The final Ge cuts were dried down, treated with concentrated HNO_3 to destroy organic compounds from the cation resin, and then re-dissolved in 2 ml 0.5 M HNO_3 for Ge isotope measurements. The Ge yields were >90 % and the total procedural blank was <1 ng and, thus, negligible for all samples. Because the Ge double spike is added prior to sample digestion, the slightly incomplete yields are inconsequential for the Ge isotope measurements.

In preparation for the chemical separation and purification for Te and Zn, the matrix cuts from both stages of the ion exchange chemistry as well as the fluorides separated prior to sample loading were combined, evaporated to dryness, and treated with HCl to destroy the fluorides and convert the samples to chloride form. Tellurium was separated from the sample matrix using a three-stage ion exchange column chromatography (Hellmann *et al.*, 2020). The samples were dissolved in 25 ml 2 M HCl and loaded onto pre-cleaned Environmental Express ion exchange columns filled with 3 ml BioRad AG1-X8 resin (200-400 mesh). The columns were then washed sequentially with 15 ml 2 M HCl, 7 ml 11 M HCl, and 15 ml 5 M HF, where Zn was eluted and collected quantitatively in the last step. Afterwards, Te was eluted in 10 ml 1 M HNO_3, followed by several dry downs in concentrated HNO_3 and conversion to chloride form through dry downs in concentrated HCl. The Te cuts were re-dissolved in 1 ml 2 M HCl and loaded onto pre-cleaned BioRad Poly-Prep columns filled 1 ml BioRad AG1-X8 resin (200-400 mesh). In the following, the columns were washed sequentially with 5 ml 2 M HCl, 2 ml 11 M HCl, and 5 ml 5 M HF, and Te was eluted using 6 ml 0.5 M HCl. After repeated dry downs in concentrated HNO_3 and HCl, the clean-up column was repeated to reduce Sb in the Te fraction sufficiently. Finally, the Te cuts were dried down in HNO_3 and HNO_3–HCl, and then dissolved in 0.28 M HNO_3 for isotope measurements.

The Zn cuts obtained from the Te chemistry were further purified following previously established ion exchange procedures (Steller *et al.*, 2022). The samples were evaporated, converted with concentrated HCl, and loaded in 10 ml 0.8 M HCl onto precleaned Biorad columns filled with 1 ml AG1-X8 resin (200-400 mesh). Remaining matrix elements were eluted with 9 ml 0.4 M HCl and 5 ml 8 M HCl, before Zn was eluted in 7 ml 0.5 M HNO_3. This chemistry was repeated once following the same procedures, except that loading was accomplished in 1 ml 0.8 M HCl and the 8 M HCl step was omitted. The final Zn cuts were dried down in HNO_3, and then dissolved in 0.3 M HNO_3 for isotope measurements.

Isotope Measurements of Ge, Te, and Zn

The Ge isotope measurements were performed on a Thermo Scientific Neoma multicollector ICP-MS at the Max Planck Institute for Solar System Research in Göttingen, following the analytical protocol of Wölfer *et al.* (2025b). Samples were introduced using a Cetac Aridus II desolvator and a Savillex C-flow nebulizer at an uptake rate of ~70 µl/min. Using standard sampler and X skimmer cones, a signal intensity of ~10 V on ^{70}Ge was obtained for an optimally spiked ~100 ppb Ge solution. Each measurement consisted of on-peak zero measurements of 20 × 8 s, followed by 50 isotope ratio measurements of 8 s each. Isobaric interferences of Zn on ^{70}Ge and of Se on ^{74}Ge and ^{76}Ge were corrected by monitoring ^{66}Zn and ^{77}Se and using the exponential mass fractionation law. Prior to each analysis, the sample introduction system was washed using 0.28 M HNO_3 for 5 min. Processing of the measured raw data was performed off-line following the three-dimensional data reduction scheme of Siebert *et al.* (2001), as described by Wölfer *et al.* (2025b). The results are shown in the $\delta^{74/70}Ge$ notation as the permil deviation of the $^{74}Ge/^{70}Ge$ ratio of a sample from the composition of the NIST SRM 3210a Ge standard:

$$\delta^{74/70}\mathrm{Ge} = \left[\frac{(^{74}\mathrm{Ge}/^{70}\mathrm{Ge})_{\mathrm{sample}}}{(^{74}\mathrm{Ge}/^{70}\mathrm{Ge})_{\mathrm{SRM3120a}}} - 1\right] \times 1000 \qquad \text{Eq. S-1}$$

The results are reported as the mean of replicate measurements and the corresponding errors are Student-t 95 % confidence intervals (95 % CI). The accuracy and reproducibility of the Ge isotope measurements were assessed by repeated analyses of the Alfa Aesar Ge solution standard and the Allende MS-A reference material, the latter of which was processed through the full chemical separation described above and analyzed together with the other chondritic samples. The measured Ge isotopic compositions of the Alfa Aesar Ge solution standard and Allende (MS-A) are $\delta^{74/70}$Ge = –0.77 ± 0.02 (95 % CI, 2 s.d. = 0.07, N = 12) (Table S-1) and $\delta^{74/70}$Ge = 0.02 ± 0.03 (95 % CI, 2 s.d. = 0.06, N = 6), respectively, and are excellent agreement with previously reported results (Wölfer *et al.*, 2025 a,b). Along the stable isotope measurements, precise bulk Ge concentrations of the samples were determined by isotope dilution.

The Te isotope measurements were performed on a Thermo Scientific Neoma multicollector ICP-MS at the Max Planck Institute for Solar System Research in Göttingen, following the analytical protocol of Hellmann *et al.* (2020). Samples were introduced using a Cetac Aridus II desolvator and a Savillex C-flow nebulizer at an uptake rate of ~50 µl/min. Using standard sampler and X skimmer cones, total ion beam intensities of ~2× 10^{-10} A were obtained for an optimally spiked ~100 ppb Te solution. Depending on the available amount of Te, samples were measured at 30-100 ppb Te (Tagish Lake and Tarda at 30 ppb Te, Orgueil and Ryugu at 50 ppb Te, Allende at 100 ppb). Each measurement consisted of on-peak zero measurements of 25 × 4 s, followed by 50 isotope ratio measurements of 4 s each. Isobaric interferences of Xe on ^{126}Te and ^{128}Te, and of Sb on ^{123}Te were corrected by monitoring ^{129}Xe and ^{121}Sb and using the exponential mass fractionation law. Prior to each analysis, the sample introduction system was washed using 0.28 M HNO_3 for 10 min. The raw data were reduced off-line following the three-dimensional data reduction scheme of Siebert *et al.* (2001), as described by Hellmann *et al.* (2020). The results are shown in the $\delta^{128/126}$Te notation as the permil deviation of the ^{128}Ge/^{126}Ge ratio of a sample from the composition of the NIST SRM 3156 Te standard:

$$\delta^{128/126}\mathrm{Te} = \left[\frac{(^{128}\mathrm{Te}/^{126}\mathrm{Te})_{\mathrm{sample}}}{(^{128}\mathrm{Te}/^{126}\mathrm{Te}_{\mathrm{SRM3156}}} - 1\right] \times 1000 \qquad \text{Eq. S-2}$$

The results are reported as the mean of pooled solution replicates (n = 3-4) with their corresponding two standard deviation (2 s.d.). Along the stable isotope measurements, precise bulk Te concentrations of the samples were determined by isotope dilution.

The Zn isotope measurements were performed using a Thermo Scientific Neoma multicollector ICP-MS at the Max Planck Institute for Solar System Research in Göttingen, broadly following previously established protocols (Steller *et al.*, 2022). Solutions containing ~200 µg/g Zn were introduced into the mass spectrometer through an Apex 2 IR with a Savillex C-flow nebulizer at an uptake rate of ~60 µl/min. At low resolution mode and with 10^{-11} Ω feedback resistors connected to the Faraday cups, this setup resulted in a total sensitivity of ~250 V per ppm of Zn. Each measurement consisted of an on-peak zero baseline measurement of 30 × 8 s, followed by 75 isotope ratio measurements of 8 s each. Isobaric interferences of Ni on ^{64}Zn, and of Ge on ^{70}Zn were corrected by monitoring ^{61,62}Ni and ^{72,73}Ge and using the exponential mass fractionation law. Prior to each analysis, the sample introduction system was washed for 2 min using 0.3 M HNO_3. The mass-dependent Zn isotopic compositions of the samples are reported in the $\delta^{66/64}$Zn notation as the permil deviation of the ^{66}Zn/^{64}Zn ratio of a sample from the composition of the NIST SRM 683 Zn bracketing standard:

$$\delta^{66/64}\mathrm{Zn} = \left[\frac{(^{66}\mathrm{Zn}/^{64}\mathrm{Zn})_{\mathrm{sample}}}{(^{66}\mathrm{Zn}/^{64}\mathrm{Zn}_{\mathrm{SRM683}}} - 1\right] \times 1000 \qquad \text{Eq. S-3}$$

To allow for a better comparison with previous literature data, the obtained $\delta^{66/64}Zn_{SRM683}$ values are normalized to the JMC Lyon Zn standard using $\delta^{66/64}Zn_{JMC,Lyon} = \delta^{66/64}Zn_{SRM683} + 0.11$ (Chen *et al.*, 2016). The mass-dependent results are reported as the mean of pooled solution replicates (n = 6–68) and the corresponding errors are two times the standard deviation (2 s.d.). The accuracy of our mass-dependent Zn measurements was tested by analyzing the AA-ETH Zn standard and the basalt standard BIR-1a processed through our chemical procedures along with the samples. We

determined a $\delta^{66/64}Zn_{JMC,Lyon}$ = 0.28 ± 0.06 (2 s.d., N = 17) for AA-ETH Zn, and 0.27 ± 0.05 (2 s.d., N = 19) for BIR-1a (Table S-1), fully consistent with the proposed best estimate value of 0.28 ± 0.02 for AA-ETH Zn (Archer *et al.*, 2017) and 0.25 ± 0.05 for BIR-1a (Wang *et al.*, 2017).

Mass-independent Zn isotope data were obtained through mass-bias correction by internal normalization to $^{67}Zn/^{64}Zn$ = 0.08216 or $^{68}Zn/^{64}Zn$ = 0.37523 and using the exponential law, respectively. The mass-independent Zn isotope data are reported in $\mu^{i}Zn$ notation the as parts per million deviation of a sample's $^{i}Zn/^{64}Zn$ ratio from that of the NIST SRM 683 Zn bracketing standard according to:

$$\mu^{i}Zn = \left[\frac{(\,^{i}Zn/^{64}Zn)_{sample}}{(\,^{i}Zn/^{64}Zn_{SRM683}} - 1\right] \times 10^{6} \qquad \text{Eq. S-4}$$

where i = 66, 67, or 68. The external reproducibility (2 s.d.) of the bracketing NIST SRM 683 standard for a given session is on average 8 and 14 ppm for $\mu^{66}Zn$ and $\mu^{68}Zn$ (normalized to $^{67}Zn/^{64}Zn$), and 6 and 10 ppm for $\mu^{66}Zn$ and $\mu^{67}Zn$ (normalized to $^{68}Zn/^{64}Zn$), respectively. The mass-independent Zn isotope results are reported as the mean of pooled solution replicates (N = 6–27) and the corresponding errors are Student-t 95 % confidence intervals (95 % CI). The accuracy and precision of the mass-independent Zn isotope data was monitored by analyzing terrestrial standards (AA-ETH Zn [N = 17] and BIR-1a [N = 19]), which returned $\mu^{i}Zn$ signatures indistinguishable from the SRM standard at the 1-ppm-level (Table S-1).

Supplementary Tables

Table S-1 Germanium and Zn isotopic data for reference materials and terrestrial standards.

Sample	N (Ge)	$\delta^{74/70}$Ge (± 95 % CI)	N (Zn)	$\delta^{66/64}$Zn (± 2 s.d.)	μ^{66}Zn (± 95 % CI)	μ^{68}Zn (± 95 % CI)	μ^{66}Zn (± 95 % CI)	μ^{68}Zn (± 95 % CI)
					^{67}Zn/^{64}Zn int. norm.		^{68}Zn/^{64}Zn int. norm.	
Ge Alfa Aesar	12	−0.77 ± 0.02						
AA-ETH Zn			17	0.28 ± 0.06	0 ± 2	0 ± 2	0 ± 1	0 ± 2
BIR-1a			19	0.27 ± 0.05	0 ± 2	1 ± 3	−1 ± 1	−1 ± 2

Table S-2 Germanium concentration and isotopic data for chondrite samples investigated in this study and comparison to literature data.

Sample	Ge (µg/g)	$\delta^{74/70}$Ge (± 95 % CI)	References
Orgueil	34.6	1.00 ± 0.04	(1)
Orgueil (this study)	33.9	1.01 ± 0.03	
Tagish Lake	27.5	0.71 ± 0.04	(1)
Tagish Lake (this study)	25.6	0.67 ± 0.03	
Tagish Lake (this study)	25.2	0.65 ± 0.03	
Tagish Lake (this study)	25.1	0.66 ± 0.04	
Tagish Lake (this study)	25.5	0.67 ± 0.02	
Tagish Lake (this study)	26.2	0.71 ± 0.03	
Tagish Lake (this study)	25.5	0.72 ± 0.02	
Tarda	24.1	0.79 ± 0.04	(1)
Tarda (this study)	24.4	0.73 ± 0.03	
Allende	16.8	-0.02 ± 0.05	(1)
Allende (this study)	17.2	0.02 ± 0.03	

References: (1) Wölfer *et al.* (2025a).

Table S-3 Tellurium concentration and isotopic data for chondrite samples investigated in this study and comparison to literature data.

Sample	Te (µg/g)	$\delta^{128/126}$Te (± 2 s.d.)	References
Orgueil	2.250	0.16 ± 0.01	(1)
Orgueil	2.190	0.20 ± 0.07	(2)
Lit. Av.	2.220	0.18 ± 0.06	
Orgueil (this study)	2.269	0.15 ± 0.02	
Tagish Lake	1.669	0.11 ± 0.01	(1)
Tagish Lake (this study)	1.729	0.13 ± 0.03	
Tagish Lake (this study)	1.764	0.12 ± 0.03	
Tagish Lake (this study)	1.556	0.12 ± 0.06	
Tagish Lake (this study)	1.647	0.10 ± 0.01	
Tagish Lake (this study)	1.756	0.12 ± 0.05	
Tagish Lake (this study)	1.691	0.11 ± 0.03	
Tarda	1.563	0.08 ± 0.01	(3)
Tarda (this study)	1.622	0.07 ± 0.07	
Allende	0.948	0.02 ± 0.02	(1)
Allende	0.939	0.02 ± 0.01	(1)
Allende	0.899	0.01 ± 0.04	(2)
Allende	0.833	0.00 ± 0.01	(2)
Lit. Av.	0.905	0.01 ± 0.02	
Allende (this study)	0.954	0.02 ± 0.02	

References: (1) Hellmann *et al.* (2020); (2) Morton *et al.* (2024); (3) Hellmann *et al.* (2023).

Table S-4 Zinc concentration and isotopic data for chondrite samples investigated in this study and comparison to literature data.

Sample	Zn (µg/g)	$\delta^{66/64}$Zn (± 2 s.d.)	References
Ryugu	361	0.43 ± 0.05	(4)
Ryugu (this study)	348	0.51 ± 0.12	
Orgueil	307	0.46 ± 0.05	(1)
Orgueil	307	0.52 ± 0.05	(1)
Orgueil	307	0.42 ± 0.09	(2)
Orgueil	303	0.45 ± 0.09	(2)
Orgueil	303	0.43 ± 0.09	(2)
Orgueil	311	0.43 ± 0.09	(2)
Orgueil	291	0.51 ± 0.09	(2)
Orgueil	272	0.45 ± 0.09	(2)
Orgueil	296	0.42 ± 0.04	(3)
Orgueil	288	0.52 ± 0.08	(4)
Lit. Av.	**299**	**0.46 ± 0.08**	
Orgueil (this study)	318	0.51 ± 0.08	
Orgueil (this study)	298	0.53 ± 0.11	
Tagish Lake	214	0.43 ± 0.05	(1)
Tagish Lake	207	0.47 ± 0.05	(1)
Tagish Lake	209	0.41 ± 0.05	(1)
Tagish Lake	209	0.47 ± 0.05	(1)
Tagish Lake	204	0.42 ± 0.06	(4)
Lit. Av.	**209**	**0.44 ± 0.06**	
Tagish Lake (this study)	196	0.51 ± 0.08	
Tagish Lake (this study)	202	0.63 ± 0.05	
Tagish Lake (this study)	188	0.52 ± 0.04	
Tagish Lake (this study)	187	0.57 ± 0.06	
Tagish Lake (this study)	197	0.53 ± 0.09	
Tagish Lake (this study)	188	0.48 ± 0.03	
Tarda	201	0.46 ± 0.07	(4)
Tarda (this study)	194	0.54 ± 0.05	
Tarda (this study)	205	0.46 ± 0.06	
Jbilet Winselwan	181	0.33 ± 0.04	(3)
Jbilet Winselwan (this study)	183	0.41 ± 0.08	
Allende	117	0.37 ± 0.05	(1)
Allende		0.32 ± 0.05	(1)
Allende	112	0.27 ± 0.04	(5)
Allende	108	0.30 ± 0.02	(5)
Allende		0.26 ± 0.12	(6)
Allende	99	0.12 ± 0.05	(3)
Allende	100	0.23 ± 0.05	(3)
Allende	110	0.22 ± 0.07	(4)
Allende	121	0.24 ± 0.06	(4)
Lit. Av.	**110**	**0.26 ± 0.14**	
Allende (this study)	111	0.31 ± 0.07	
Allende (this study)	108	0.27 ± 0.08	
Vigarano	116	0.28 ± 0.05	(1)
Vigarano (this study)	104	0.17 ± 0.05	

References: (1) Luck *et al.* (2005); (2) Barrat *et al.* (2012); (3) Morton *et al.* (2024); (4) Paquet *et al.* (2023); (5) Pringle *et al.* (2017); (6) Makishima and Nakamura (2013).

Supplementary Figures

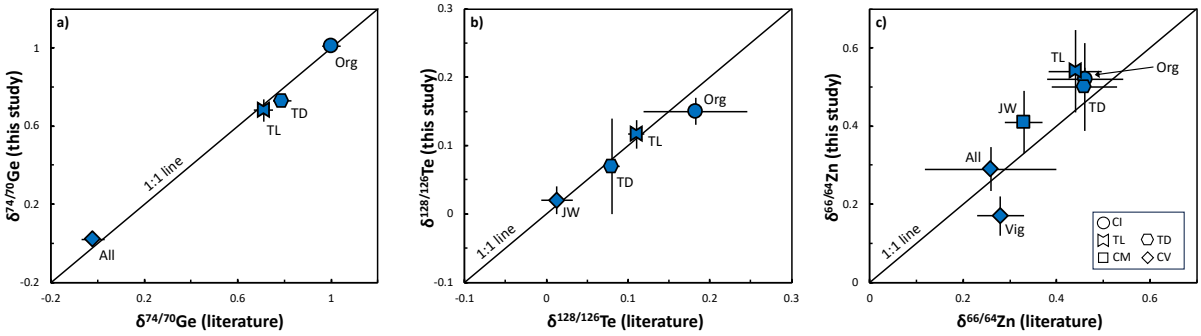

Figure S-1 Diagrams of the **(a)** Ge, **(b)** Te, and **(c)** Zn mass-dependent isotopic compositions of carbonaceous chondrites reported in the literature in comparison to the results of this study. Each point represents the average composition of a given sample. Stated uncertainties represent two times the standard deviation (2 s.d) in case of Te and Zn, and 95 % confidence intervals (95 % CI) in case of Ge. Individual literature data are reported in Tables S-2 to S-4.

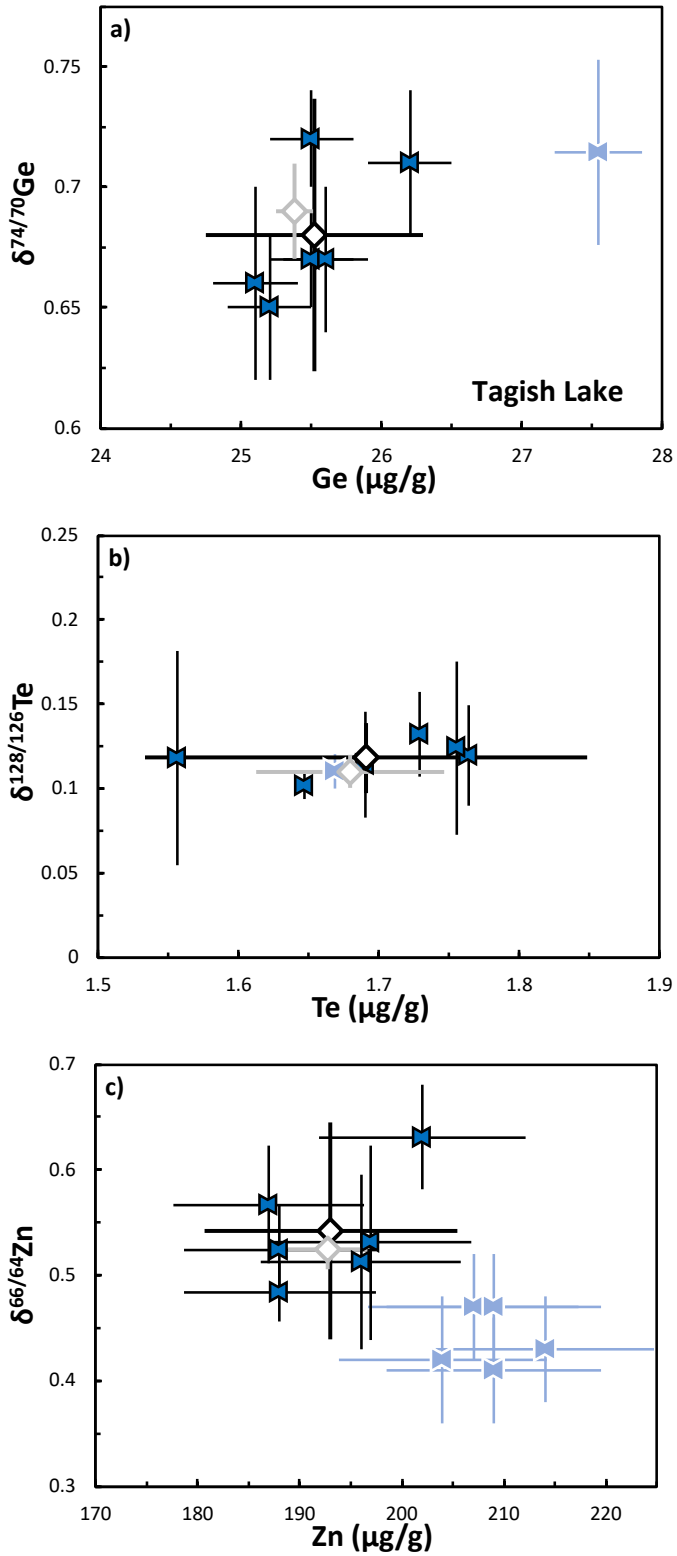

Figure S-2 Diagrams of **(a)** Ge concentrations vs. $\delta^{74/70}$Ge variations, **(b)** Te concentrations vs. $\delta^{128/126}$Te variations, and **(c)** Zn concentrations vs. $\delta^{66/64}$Zn variations of Tagish Lake (data from this study in dark blue [average (2 s.d.) in black; weighted mean in grey]; literature data in light blue). Literature data for Ge is from Wölfer *et al.* (2025a); data for Te is from Hellmann *et al.* (2020).

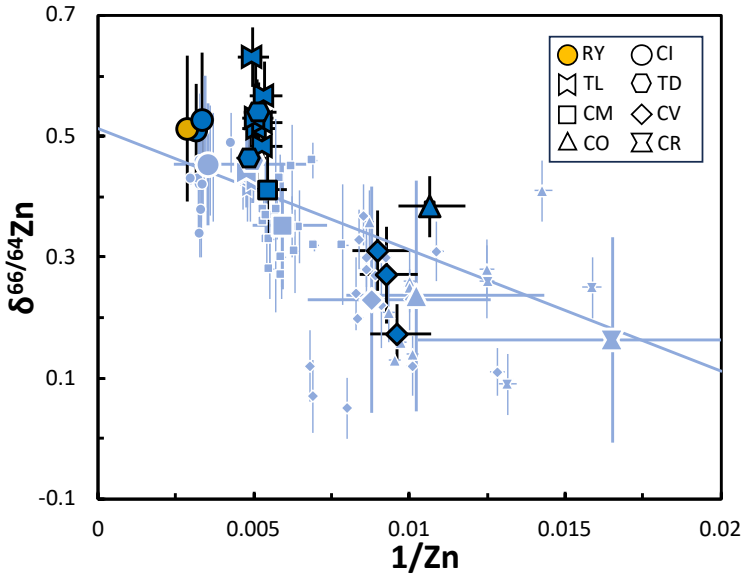

Figure S-3 Diagram of 1/Zn vs. $\delta^{66/64}$Ge variations of carbonaceous chondrites (data from this study in dark blue; literature data in light blue [small symbols represent individual samples; large symbols represent the group averages]) and Ryugu sample A0220 (orange circle). Literature data are from Luck *et al.* (2005), Barrat *et al.* (2012), Pringle *et al.* (2017), Mahan *et al.* (2018), Paquet *et al.* (2023), and Morton *et al.* (2024). All Zn isotope data are shown relative to the JMC Lyon reference standard. The blue line represents the weighted regression calculated using IsoplotR and is based on the group averages compiled from the literature.

Supplementary Information References

Archer, C., Andersen, M.B., Cloquet, C., Conway, T.M., Dong, S. *et al.* (2017) Inter-calibration of a proposed new primary reference standard AA-ETH Zn for zinc isotopic analysis. *Journal of Analytical Atomic Spectrometry* 32, 415–419. https://doi.org/10.1039/C6JA00282J

Barrat, J.A., Zanda, B., Moynier, F., Bollinger, C., Liorzou, C., Bayon, G. (2012) Geochemistry of CI chondrites: Major and trace elements, and Cu and Zn Isotopes. *Geochimica et Cosmochimica Acta* 83, 79–92. https://doi.org/10.1016/j.gca.2011.12.011

Chen, S., Liu, Y., Hu, J., Zhang, Z., Hou, Z., Huang, F., Yu, H. (2016) Zinc Isotopic Compositions of NIST SRM 683 and Whole-Rock Reference Materials. *Geostandards and Geoanalytical Research* 40, 417–432. https://doi.org/10.1111/j.1751-908X.2015.00377.x

Hellmann, J.L., Hopp, T., Burkhardt, C., Kleine, T. (2020) Origin of volatile element depletion among carbonaceous chondrites. *Earth and Planetary Science Letters* 549, 116508. https://doi.org/10.1016/j.epsl.2020.116508

Hellmann, J.L., Schneider, J.M., Wölfer, E., Drążkowska, J., Jansen, C.A., Hopp, T., Burkhardt, C., Kleine, T. (2023) Origin of Isotopic Diversity among Carbonaceous Chondrites. *The Astrophysical Journal Letters* 946, L34. https://doi.org/10.3847/2041-8213/acc102

Luais, B. (2007) Isotopic fractionation of germanium in iron meteorites: Significance for nebular condensation, core formation and impact processes. *Earth and Planetary Science Letters* 262, 21–36. https://doi.org/10.1016/j.epsl.2007.06.031

Luais, B. (2012) Germanium chemistry and MC-ICPMS isotopic measurements of Fe–Ni, Zn alloys and silicate matrices: Insights into deep Earth processes. *Chemical Geology* 334, 295–311. https://doi.org/10.1016/j.chemgeo.2012.10.017

Luck, J.-M., Othman, D.B., Albarède, F. (2005) Zn and Cu isotopic variations in chondrites and iron meteorites: Early solar nebula reservoirs and parent-body processes. *Geochimica et Cosmochimica Acta* 69, 5351–5363. https://doi.org/10.1016/j.gca.2005.06.018

Mahan, B., Moynier, F., Beck, P., Pringle, E.A., Siebert, J. (2018) A history of violence: Insights into post-accretionary heating in carbonaceous chondrites from volatile element abundances, Zn isotopes and water contents. *Geochimica et Cosmochimica Acta* 220, 19–35. https://doi.org/10.1016/j.gca.2017.09.027

Makishima, A., Nakamura, E. (2013) Low-blank chemistry for Zn stable isotope ratio determination using extraction chromatographic resin and double spike-multiple collector-ICP-MS. *Journal of Analytical Atomic Spectrometry* 28, 127–133. https://doi.org/10.1039/C2JA30271C

Morton, E.M., Pickard, H., Wombacher, F., Huang, Y., Palk, E., Martins, R., Kuthning, S., Schönbächler, M., Rehkämper, M. (2024) Volatile Element Depletion of Carbonaceous Chondrites—Insights from Mass-dependent Zinc, Cadmium, and Tellurium Isotope Variations. *The Astrophysical Journal* 977, 53. https://doi.org/10.3847/1538-4357/ad87ed

Paquet, M., Moynier, F., Yokoyama, T., Dai, W., Hu, Y. *et al.* (2023) Contribution of Ryugu-like material to Earth's volatile inventory by Cu and Zn isotopic analysis. *Nature Astronomy* 7, 182–189. https://doi.org/10.1038/s41550-022-01846-1

Pringle, E.A., Moynier, F., Beck, P., Paniello, R., Hezel, D.C. (2017) The origin of volatile element depletion in early solar system material: Clues from Zn isotopes in chondrules. *Earth and Planetary Science Letters* 468, 62–71. https://doi.org/10.1016/j.epsl.2017.04.002

Schneider, J.M., Burkhardt, C., Kleine, T. (2023) Distribution of *s*-, *r*-, and *p*-process Nuclides in the Early Solar System Inferred from Sr Isotope Anomalies in Meteorites. *The Astrophysical Journal Letters* 952, L25. https://doi.org/10.3847/2041-8213/ace187

Siebert, C., Nägler, T.F., Kramers, J.D. (2001) Determination of molybdenum isotope fractionation by double-spike multicollector inductively coupled plasma mass spectrometry. *Geochemistry, Geophysics, Geosystems* 2, 2000GC000124. https://doi.org/10.1029/2000GC000124

Steller, T., Burkhardt, C., Yang, C., Kleine, T. (2022) Nucleosynthetic zinc isotope anomalies reveal a dual origin of terrestrial volatiles. *Icarus* 386, 115171. https://doi.org/10.1016/j.icarus.2022.115171

Tachibana, S., Sawada, H., Okazaki, R., Takano, Y., Sakamoto, K. *et al.* (2022) Pebbles and sand on asteroid (162173) Ryugu: In situ observation and particles returned to Earth. *Science* 375, 1011–1016. https://doi.org/10.1126/science.abj8624

Wang, Z.-Z., Liu, S.-A., Liu, J., Huang, J., Xiao, Y., Chu, Z.-Y., Zhao, X.-M., Tang, L. (2017) Zinc isotope fractionation during mantle melting and constraints on the Zn isotope composition of Earth's upper mantle. *Geochimica et Cosmochimica Acta* 198, 151–167. https://doi.org/10.1016/j.gca.2016.11.014

Wölfer, E., Burkhardt, C., Nimmo, F., Kleine, T. (2025a) Origin of moderately volatile elements in Earth inferred from mass-dependent Ge isotope variations among chondrites. *Earth and Planetary Science Letters* 663, 119435. https://doi.org/10.1016/j.epsl.2025.119435

Wölfer, E., Burkhardt, C., Kleine, T. (2025b) Germanium stable isotope measurements by double-spike MC-ICPMS. *Journal of Analytical Atomic Spectrometry* 40, 1023–1036. https://doi.org/10.1039/D4JA00359D

Yada, T., Abe, M., Okada, T., Nakato, A., Yogata, K. *et al.* (2022) Preliminary analysis of the Hayabusa2 samples returned from C-type asteroid Ryugu. *Nature Astronomy* 6, 214–220. https://doi.org/10.1038/s41550-021-01550-6